Applied Catalysis B: Environmental 125 (2012) 516–529

Contents lists available at SciVerse ScienceDirect

Applied Catalysis B: Environmental

journal homepage: www.elsevier.com/locate/apcatb

A comparison of sol–gel and impregnated Pt or/and Ni based γ-alumina catalysts for bioglycerol aqueous phase reforming

M. El Doukkali [a,*], A. Iriondo [a], P.L. Arias [a], J. Requies [a], I. Gandarías [b], L. Jalowiecki-Duhamel [b], F. Dumeignil [b,c]

[a] University of Basque Country UPV/EHU, Engineering School, C/Alameda Urquijo s/n, 48013 Bilbao, Spain
[b] Université des Sciences et Technologies de Lille, CNRS UMR8181, Unité de Catalyse et de Chimie du Solide, UCCS, F-59655 Villeneuve d'Ascq Cedex, France
[c] Institut Universitaire de France, Maison des Universités, 10, Boulevard Saint-Michel, 75005 Paris, France

ARTICLE INFO

Article history:
Received 21 April 2012
Received in revised form 20 June 2012
Accepted 22 June 2012
Available online 1 July 2012

Keywords:
Platinum-nickel catalysts
Sol–gel method
Aqueous phase reforming
Bioglycerol
Hydrogen

ABSTRACT

Two series of Pt or/and Ni-based γ-alumina catalysts were prepared using sol–gel and conventional impregnation methods. Their activities were tested in the aqueous phase reforming of glycerol. All catalysts were also characterized by different techniques such as: ICP, BET, TPR-H_2, in situ XPS and XRD to study their textural and physicochemical properties. The effect of preparation method, nature of active phase and possible cooperative effect between Pt and Ni in catalytic performance have been the focus of this investigation. The results obtained showed that sol–gel catalysts present better catalytic properties. TPR-H_2, XPS and XRD showed that sol–gel PtNiAl catalyst contain well dispersed active phases and present high resistance against sintering leading to better and more stable catalytic activities, especially at moderate temperature/pressure conditions. As a result, sol–gel PtNi catalysts allowed higher reforming rates (3–8 times) to gaseous products than PtNi catalysts prepared by incipient wetness impregnation. This better behavior can be explained by the enhancement of textural properties, higher active phases dispersion and cooperative effect between Pt and Ni elements.

1. Introduction

Hydrogen is considered as an important energy vector for the 21st century. It is one of the candidates to partially replace the current main transport energy vectors (oil based), and at the same time, hydrogen can be generated, stored and used in situ for the generation of power and heat on demand. In addition to this, hydrogen production from renewable energy sources, as biomass, is an important route to achieve carbon dioxide zero emissions [1,2]. Current processes for transformation of biomass into hydrogen, such as gasification and/or steam reforming, involve high temperatures and many side reactions, which decrease the hydrogen selectivity [3,4]. In such a context, bioalcohols aqueous-phase reforming (APR) for hydrogen production presents attractive advantages, hence they have been recently reviewed by different authors [4–8].

The APR process of oxygenated compounds derived from bioalcohols to produce hydrogen was studied by Dumesic and co-workers. Thereafter this process has received considerable attention; due to its several advantages as compared to other reforming processes [8–10]. It can be carried out at relatively low temperatures (200–280 °C) and at moderated pressure (15–70 bars). Besides that as it operates in liquid phase the aqueous solution used as process feed must not be evaporated, therefore the corresponding energy saving is an attractive advantage. In addition, undesirable decomposition reactions can be limited. Furthermore, it is possible to generate H_2 and CO_2 in a simple one step reaction process with very low CO contents. The product mixture could be purified through direct transfer to membrane systems taking advantage of the reaction pressure; facilitating its use in PEM fuel cell applications. This technology can also generate 15 times more hydrogen per mass of catalyst than existing steam reforming processes [8–12].

Many oxygenated compounds, such as ethanol, ethylene glycol, sorbitol and glycerol, have been used as feeds for APR processes [8–13]. Bioglycerol is the major by-product from biodiesel production, and possible overproduction of this product favors the development of glycerol conversion alternatives [14–16]. Biodiesel is produced from vegetable oils or animal fats transesterification. Triglycerides react with methanol or ethanol to methyl- or ethyl- esters of fatty acids, as shown in Eq. (1), and glycerol is the main by-product. One ton of biodiesel production generates about 110 kg of crude bioglycerol. As biodiesel production is increasing in some countries, crude bioglycerol is also produced there in large

* Corresponding author. Tel.: +34 946017297; fax: +34 946014179.
E-mail address: mohamed.eldoukkali@ehu.es (M. El Doukkali).

0926-3373/$ – see front matter © 2012 Elsevier B.V. All rights reserved.
http://dx.doi.org/10.1016/j.apcatb.2012.06.024

amounts. To improve the biodiesel profitability, one of the promising alternatives to be considered is to convert this bioglycerol in higher added value products as biohydrogen by APR.

$$\text{Triglycerides} + 3(\text{R—OH}) \rightarrow \text{glycerol} + 3(\text{methyl/ethylesters}) \quad (1)$$

The glycerol APR process occurs according to the following global stoichiometric reaction:

$$C_3H_8O_3 + 3H_2O \rightarrow 7H_2 + 3CO_2 \quad (2)$$

The following two reactions can occur during the APR process:

$$\text{C—C/C—H bonds cracking of glycerol} : C_3H_8O_3 \rightarrow 4H_2 + 3CO \quad (3)$$

$$\text{Water-gas shift (WGS)} : CO + H_2O \rightarrow CO_2 + H_2 \quad (4)$$

The above-mentioned C—C/C—H cleavage (3), WGS (4), as well as methanation, and Fischer–Tropsch reactions are catalyzed by different metals and supports. The C—C/C—H scission, activated by metallic sites, leads to H_2 and CO_2, while the C—O cleavage, facilitated by catalyst acid sites, leads to produce diols, monoalcohols, and alkanes [17]. Beside, the CO and/or CO_2 react with H_2 would lead to alkanes by methanation or Fischer–Tropsch reactions, decreasing as a consequence the hydrogen yield. Apart from the reactions already mentioned for the reforming of glycerol into light gaseous products, further reactions are feasible in the aqueous phase at low temperatures such as dehydrogenation (5) and dehydration/hydrogenation of glycerol to diols or other oxygenated compounds (6).

$$\text{Dehydrogenation of glycerol} : C_3H_8O_3 \leftrightarrow C_3H_6O_3 + H_2 \quad (5)$$

$$\text{Dehydration/Hydrogenation} : C_3H_8O_3 + H_2 \leftrightarrow C_3H_8O_2 \rightarrow 4H_2O + 3CO \quad (6)$$

An active APR catalyst should not only be active for the cleavage of the C—C/C—H bonds, but also for the water-gas shift (WGS) reaction. Moreover, the catalyst should be inert to parallel and series competing reactions such as the cleavage of the C—O bond, methanation and the Fischer–Tropsch reactions which greatly decrease the H_2 yield [8–12]. To achieve this goal, there are clear incentives to develop new active and selective catalysts for APR catalytic process as it is intended in this work. Recently, sol–gel procedure has been proposed as a new preparation method of γ-Al_2O_3 supported metal catalyst. The γ-Al_2O_3 phase was chosen in this work because it presents large specific surface areas, well-defined pore size distributions and stability within a wide temperature range [18]. It is also able to stabilize and disperse the active phases adequately, showing as well a moderate acidity [19]. Usually sol–gel catalysts based on γ-Al_2O_3 are prepared from a homogenous solution containing both the metals and the support precursors. In several papers it has been shown that these catalysts [20–23] allow high active phase dispersion, high thermal resistance to sintering, and low deactivation rates, if they are compared to catalysts prepared using more conventional impregnation methodologies. A variety of catalyst formulations based on precious metal and non-precious metals have been described in different papers [1,12,13,17,24–31]. The precious metal catalysts, such as Pt based ones, have shown the best performances. It has also been reported that Re addition to Pt improves significantly catalytic activity [30,31]. Nevertheless, Ni phases are widely used due to their low cost and high availability, and also due to their high activity for C—C bond cleavage. Alloying of Pt with Ni or Co has also been studied. In this work the influence of Ni on Pt catalysts will be considered as a cheaper alternative.

In order to fulfill this objective, γ-alumina Pt, Ni and PtNi-based catalysts were chosen as promising candidates for glycerol APR. Two series of Pt, Ni and PtNi catalysts supported on γ-Al_2O_3 were prepared, one by sol–gel method under basic conditions (SGB), and the other one by incipient wetness impregnation (IWI). In addition, a detailed characterization of all the prepared samples was carried out to examine their textural and physicochemical properties. Their catalytic activities were tested at two different temperatures/pressures (230 °C/30 bar and 250 °C/50 bar) in the aqueous phase reforming of glycerol/water mixture (10 wt%) trying to maximize hydrogen production. The aim was to study the influence of the preparation method on Pt, Ni and PtNi on γ-Al_2O_3 catalytic properties. The influence of the reaction conditions was also studied. In fact, the space velocity and catalyst mass were increased as compared to the ones used in a previous work [31]. The main goal of this work is to reach really high glycerol conversions toward gaseous products, especially toward hydrogen, but the quantity and distribution of other products was also considered.

2. Experimental

2.1. Materials and catalyst preparation

For comparative purposes, supported Pt, Ni and PtNi on γ-Al_2O_3 catalysts were prepared by IWI method [1,17,31–33]. As support, a commercial γ-Al_2O_3 (Merck, 99.5%, S_{BET} = 140 m^2/g) was used along with aqueous solutions of $H_2PtCl_6{\cdot}xH_2O$ (Sigma–Aldrich, 99.99%) or/and $Ni(NO_3)_2{\cdot}6H_2O$ (Sigma–Aldrich, 99.99%). The metal concentrations in the precursor solutions were adjusted to obtain 3 wt% of Pt and 10 wt% of Ni. The solid support and solution was kept at room temperature during 2 h with gentle shaking. Then, at first removal of water was carried out using a rota-vapor at 70 °C and under mechanical vacuum. Moreover, another series of γ-alumina based Pt, Ni and PtNi, were prepared by sol–gel method under basic conditions (SGB) [17–19]. First, aluminum isopropoxide (AIP) $Al[OCH(CH_3)_2]_3$ (Sigma–Aldrich 99.995%) was hydrolyzed at 40 °C using a molar ratio H_2O/AIP = 100. This solution was then peptized adding NH_4OH. The pH of this hydrolyzed solution was adjusted to 10.3. Secondly, other solution was prepared dissolving the metal precursor salt of the active phase in absolute ethanol. This salt solution was added to the AIP-derived alumina sol at 40 °C and the mixture was vigorously stirred. After this, the sol formed was placed in ultrasound during 30 min. The alcoholic solvent was removed by drying at 40 °C during 24 h. The impregnated solids obtained by IWI and the spongy material obtained by SGB were dried under air at 100 °C overnight, and subsequently calcined at 550 °C (2 °C/min) for 6 h under an air flow of 2 L min^{-1} $g_{cat.}{}^{-1}$.

2.2. Catalyst characterization

The elemental, textural and structural properties of calcined and reduced catalysts were characterized by different techniques. The calcined catalysts were characterized by inductively coupled plasma atomic emission spectroscopy (ICP-AES), isotherms of N_2 adsorption/desorption at 77 K, temperature programmed reduction (TPR-H_2), X-ray powder diffraction (XRD) and X-ray photoelectron spectroscopy (XPS). To analyze the changes in its physicochemical properties just before starting the APR reaction, all catalysts were reduced in situ inside a XRD and XPS chambers using similar treatments conditions as the employed in the APR catalytic tests. The spent PtNi catalysts were also characterized by XRD/XPS techniques to examine the changes in their properties suffered during the APR reaction.

The metal loadings in the catalysts were determined by ICP-AES, using a PerkinElmer Optima 3300DV apparatus. The samples, around 100 mg, were first dissolved in an acid solution mixture [HNO_3 (3 mL), HCl (2 mL) and HF (3 mL),] using a microwave furnace with temperature profile (7 °C/min up to 180 °C) for 45 min.

The solution obtained was diluted to concentrations within the detection range of the instrument.

The textural characteristics were evaluated employing N_2 adsorption/desorption technique at 77 K in an Autosorb-1C instrument. Prior to the analysis the samples were outgassed for 12 h at 150 °C. Specific areas were calculated from these isotherms using the BET method and taking a value of 0.162 nm^2 for the cross-section of the physically adsorbed N_2 molecule. Pore distribution and pore volume were estimated using the BJH method (desorption data).

The reducibility of the catalysts was analyzed by temperature programmed reduction (TPR-H_2), carried out in the same Quantachrome apparatus (Autosorb-1C equipped with a TCD detector). Prior to reduction experiments, the samples, around 50 mg, were thermally treated under a He stream at 300 °C to remove water and other contaminants. TPR-H_2 profiles were obtained heating the samples under a 10 vol.% H_2/Ar flow (50 mL/min) from 25 to 1000 °C at a linearly programmed rate of 10 °C/min. The effluent gas passed through a cold trap to remove water before measuring the amount of hydrogen consumed during reduction by the TC detector.

The X-ray powder diffractograms of calcined catalysts were recorded with a D 5000 Siemens diffractometer (D 8 Advance Bruker AXS) using a copper target ($\lambda_{CuK\alpha1}$ = 1.5418 Å) and a secondary beam monochromator. The analyses of reduced samples were carried out using another D 5000 Siemens diffractometer equipped with chamber analysis (Anton Paar XRK900) designed for in situ treatment by temperature and under a reducing gas (H_2/N_2). Both apparatus worked with the X-ray tubes at 40 kV and 40 mA. These beams can detect crystalline phases with an average minimum size around 2 nm. The measurements were carried out from 10° to 80° (2θ) with 0.04°/s of acquisition time for calcined and in situ reduced sample. The reduction treatment was carried out in situ at 350 °C for Pt catalysts and 750 °C for Ni and PtNi catalysts. The conditions of the reduction treatment applied are similar to those used in the catalytic tests of this research work (see Section 2.3).

The crystallite size values were obtained using the Scherrer equation:

$$D = \frac{K\lambda}{\sqrt{(\beta^2 - S^2)}\cos\theta\beta} \quad (7)$$

where D is the apparent crystallite size, K is the geometric factor (0.9 for spherical crystallites), λ is the wavelength of the radiation (1.5418 Å), S is the instrument line broadening corrected with a LaB6 reference sample, β is the reflection width at half-maximum intensity (FWHM), and θ_β is the angle corresponding to the maximum intensity of the peak. The unit cell parameters were determined by a computer program (EVA-Fit.exe v1.3-1992) using the least-square method. The θ experimental values and the reflection planes ($h\,k\,l$) were employed to obtain the unit cell.

X-ray photoelectron spectra were recorded using a Kratos Axis Ultra-DLD electron spectrometer equipped with an Al-Kα dual anode X-ray source (1486.6 eV) and a hemispherical electron analyzer operating at constant transmission energy (40 eV). The apparatus worked with a 160 W power, 10^5 mA and 15 kV. Binding energy (BE) values were referred to the C1s peak (284.6 eV) for the calcined and reduced catalysts. The Al2p peak corresponding to γ-Al_2O_3 took place at 74.5 eV (accuracy within ± 0.5 eV). The C1s, O1s, Al2p, Al2s, Pt4d and Ni2p core-level spectra were recorded. The superficial quantification was carried out by the level Al2s to avoid the influence of overlap between the peak of Pt4f and Al2p. The calcined samples were outgassed at 10^{-8} bar and transferred immediately to the ion pumped analysis chamber, whose residual pressure was kept below 7–9 × 10^{-12} bar during data acquisition. For the reduced catalysts analysis, the calcined samples, lightly pressed on a quartz-holder, were applied to a sample rod; this allowed an in situ reduction treatment with similar conditions to those used in the catalytic tests (see Section 2.3). This step was performed in the preparation chamber of the spectrometer, directly connected to the ultra-high vacuum analysis system. The measurements were carried out without significant time delays. The decomposition of the experimental photo peaks was done using the software "CasaXPS". The areas of the peaks were estimated by calculating the integral of each peak after subtracting a Shirley background and fitting the experimental peak to a combination of Lorentzian/Gaussian lines of variable proportions. The atomic relative contents were calculated from the normalized area of the corresponding photo peaks.

2.3. Experimental setup for measurements

The catalytic activity of all catalysts was evaluated by aqueous phase reforming of a glycerol/water mixture ($C_3H_8O_3/H_2O$) using a Micro-activity modular laboratory system (PID Eng. & Tech.). A schematic of the experimental setup is provided in Fig. 1.

In order to avoid preferential flow paths and hot spots, 1 g of catalyst (particle size of 0.42–0.50 mm) were diluted with SiC 0.6 mm diameter (1:3, w/w). Prior to catalytic tests, the catalysts were heated for 90 min under 150 mL/min of N_2 up to the desired reduction temperature (T_R). Immediately, the catalyst was reduced under 100 mL/min of H_2/N_2 mixture (75 vol.% H_2) for 2 h at 350 °C for Pt catalysts and at 750 °C for Ni and PtNi catalysts. After purging the system with N_2 to remove the remaining H_2 and the H_2O formed during the reduction treatment, and cooling down to the reaction temperature (230 °C/250 °C), the backpressure regulator was set at the desired pressure (30/50 bar), passing the N_2 through a Peltier separator. After the system reached its stability, the aqueous feed solution comprising 10% glycerol (by weight) was introduced using a HPLC digital pump at a flow rate of 0.4 mL/min (experimental WHSV was around 2.6 h^{-1}). The reagent mixture was fed into the fixed-bed reactor from bottom to top in order to improve its contact with the catalyst. The feed composition was similar to the glycerol content obtained from biodiesel production after alcohol removal and acid neutralization of the glycerol fraction [16]. The activity measurements of all catalysts were carried out under thermodynamic condition in which the reactant mixture is a liquid phase. In addition, to avoid any mixture of N_2 (used to drag the gaseous products of the Peltier) with the reactants in the reactor a "non-return valve" was placed at the inlet of the Peltier (see apparatus setup in Fig. 1).

Exhausted gases were periodically sampled and analyzed with an on-line μGC/SM. The oxygenated hydrocarbon compounds (OHCs), such as: 2-propanol, 1,2-propanediol, ethylene glycol, acetol, acetic acid, methanol and non-reacted glycerol, were condensed at 15 °C (vapor–liquid condenser) and analyzed by GC. The product distribution was monitored along 32 h on stream. Catalytic activity was evaluated in terms of glycerol conversion, conversion into gas, selectivity of H_2 and alkanes, total gas flow rate, H_2/CO_2 molar ratio as well as yield of OHCs. These parameters were calculated by a N_2 internal standard-based analytical method. In this paper, the results are presented according to the following expressions [9,30–33]:

Glycerol conversion:

$$GC(\%) = \frac{N^{in}_{Glycerol}(mol/min) - N^{out}_{Glycerol}(mol/min)}{N^{in}_{glycerol}(mol/min)} \times 100 \quad (8)$$

Conversion into gas:

$$CIG\,(\%) = \frac{C_{atoms\,in\,gas\,products}\,(mol/min)}{C_{atoms\,in\,feed}(mol/min)} \times 100 \quad (9)$$

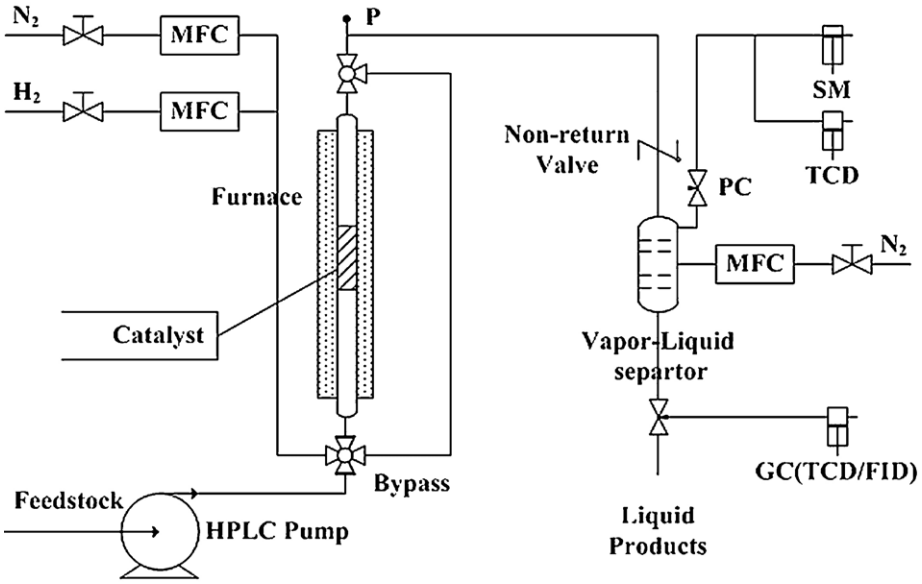

Fig. 1. Schematic design of experimental setup for APR measurements.

Flow of total gas formation:

$$F_T(\text{mL(STP)}min^{-1}g_{\text{cat.}}^{-1}) = \frac{\text{measured volume (mL)}}{\text{time(min)} \times m_{\text{cat.}}(\text{g})} \times \frac{273\ \text{K}}{T_{\text{ambient}}} \quad (10)$$

Selectivity of H_2 and alkanes:

$$S_{(i)}(\%) = \frac{N_{(i)}^{\text{out}}(\text{mol/min})}{N_{\text{C in gas phase}}^{\text{out}}(\text{mol/ min})} \times 100 \quad (11)$$

where (i) are H_2 or alkane products such as: CH_4, C_2H_6 and C_3H_8. Moreover, the H_2 selectivity is multiplied by 3/7, taking into account the occurrence of the WGS reaction after the decomposition of glycerol (3)–(4).

Yield of oxygenated hydrocarbon compounds (OHCs):

$$\text{Yield\_OHCs (j)} = \frac{N_{\text{liquid products}}^{\text{out}}(\text{mol/ min})\,(\text{exp.})}{N_{\text{glycerol}}^{\text{in}}(\text{mol/ min})} \quad (12)$$

(j) species are 2-propanol, 1,2-propanediol, ethylene glycol, acetol, acetic acid or methanol.

3. Results

3.1. Chemical composition and textural characterization by adsorption/desorption of N_2 at 77 K

The chemical composition determined by ICP-AES is shown in Table 1. The ICP results show that, in general, the samples are quite homogeneous and the weight loadings are relatively near the nominal intended values for the Pt and Ni loadings, indicating the effectiveness of both procedures used to incorporate these metal phases.

Independently of the preparation method, each series showed similar profiles of N_2 adsorption/desorption, since textural properties of catalysts are mainly related to the support properties. That is why in Fig. 2(a and b) only the curves of supports are presented, while the data of all catalysts are summarized in Table 1.

Both catalyst supports (Fig. 2(a)) showed type IV isotherms characteristic of mesoporous materials according to IUPAC classification. The relationship between the isotherms shape and pore structure was reported elsewhere [34,35]. Each support isotherm presented the corresponding hysteresis loop. The SGB support presented a hysteresis loop (Type H_2), which closes at a slightly higher pressure indicating a more developed mesoporous texture [36]. This sample is characterized by ink-bottle type pores with a plateau at the high pressure (P/P_0) range, and asymmetrical triangular form. Generally, these forms are assigned to porous systems with pore network connectivity [37]. The IWI support presented a large hysteresis loop (Type H_3) in the range $P/P_0 = 0.45$–0.99. This is typical characteristic of slit-shaped pores (stacked plane) with relative large sizes. The pore size distribution was derived from the desorption data using the Barret–Joyner–Halenda (BJH) method. The IWI pore size distribution is a little broader and centered at 5.2 nm, while one of the SGB support is narrower and centered at 4.0 nm, indicating that this support contains a better defined mesoporous structure than the IWI support. This difference is due to the method of preparation, since the basic agent added (to control the pH of the medium) generated an increase in condensation and led to clusters formation. These clusters are characterized by a spherical shape and facilitate the development of a very spongy material. This explains the textural differences observed when both alumina supports are compared [38,39].

The specific surface area and pore volume data of all samples are also shown in Table 1. The experimental data can be fitted with

Table 1
Symbol, chemical and textural characteristics of prepared systems.

Symbol	Catalyst formulas	Loading metal		Textural properties	
		Pt	Ni	S_{BET}	V_p
$Al^{(IWI)}$	γ-Al_2O_3 (com.)	–	–	140	0.23
$Al^{(SGB)}$	γ-Al_2O_3 (AIP)	–	–	375	0.43
$PtAl^{(IWI)}$	Pt/γ-Al_2O_3	3.3	–	130	0.22
$PtAl^{(SGB)}$	Pt/γ-Al_2O_3	2.2	–	339	0.40
$NiAl^{(IWI)}$	Ni/γ-Al_2O_3	–	9.6	110	0.19
$NiAl^{(SGB)}$	Ni/γ-Al_2O_3	–	9.8	319	0.38
$PtNiAl^{(IWI)}$	PtNi/γ-Al_2O_3	3.0	9.9	104	0.20
$PtNiAl^{(SGB)}$	PtNi/γ-Al_2O_3	2.6	12.6	305	0.37

The units are: metal loading → wt%, S_{BET} → $m^2/g_{cat.}$ and V_p → cm^3/g.
Com. and AIP → represent commercial γ-Al_2O_3 and aluminum isopropoxide, respectively.
IWI and SGB → represent incipient wetness impregnation and sol–gel method in basic medium, respectively.

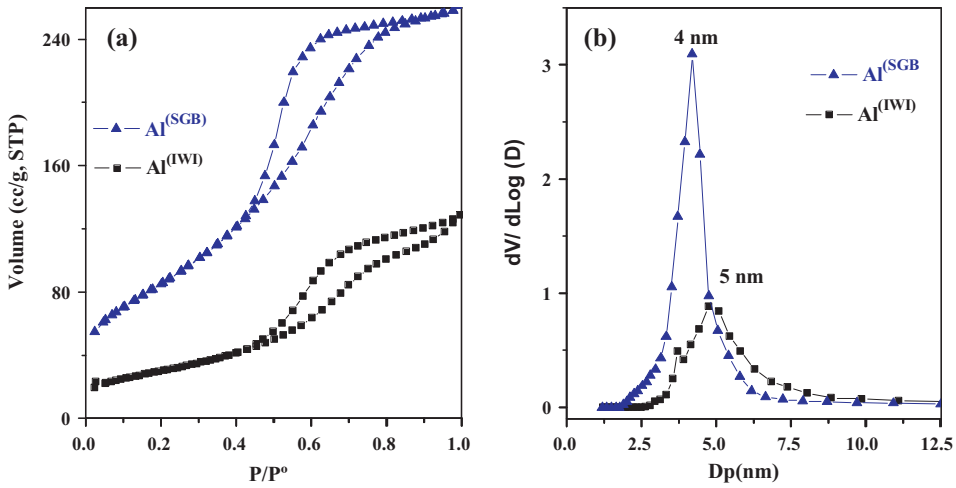

Fig. 2. N_2 adsorption/desorption isotherms at 77 K (a) and desorption data of BJH pore size distribution (b) of bulk γ-Al_2O_3 prepared by IWI and SGB methods.

excellent agreement to the well-known BET equation (correlation coefficient > 0.999), in the relative pressure range between 0.05 and 0.25. As it can be observed in this table, the Pt or/and Ni incorporation by both methods significantly reduced the surface area. This reduction is more pronounced when both metals were incorporated, because the metals amount is higher. The pore volume was slightly decreased for SGB catalysts but it was not significantly altered for IWI catalysts. This observation suggests that sol–gel method was able to incorporate part of Pt and Ni within matrix pores, leading to pore volume decrease but in the impregnated catalyst, it seems that these metals were preferentially deposited on the outer surface of the alumina.

The preparation method also provided different surface areas; the SGB prepared samples showed higher specific area than those prepared by IWI, as expected sol–gel procedures are currently under study because they allow the preparation of high surface area materials [40]. In this sense, the SGB catalysts showed a surface area approximately 3 times higher than the IWI catalysts. The catalysts prepared by SGB showed pore volumes 2 times higher than their counterparts prepared by IWI, since this property is directly related to support properties. It can be concluded that the preparation method played an important role to determine the textural properties of each series of catalysts prepared.

3.2. Temperature programmed reduction results

TPR-H_2 measurements were carried out to investigate the reducibility of the fresh catalysts and to examine the interaction among Pt or/and Ni with γ-Al_2O_3 supports. Fig. 3 shows the TPR-H_2 profiles of the Pt, Ni and PtNi catalysts prepared by IWI (a) and SGB (b) methods. As it can be seen there, all Pt-containing catalysts presented reduction peak between 100 and 300 °C, approximately. According to the literature [41], these peaks could be ascribed to the reduction of PtO_x species interacting with the oxygen atoms of γ-Al_2O_3. The presence of these species could then be related to the capacity of the γ-Al_2O_3 to stabilize oxidized Pt particles over its surface [42]. It can be remarked that the SGB catalysts presented broader TPR peaks at lower temperatures than IWI samples.

TPR-H_2 profiles of Ni monometallic catalysts presented different types of reduction peaks corresponding to nickel species in different environments and showing different interaction degrees with γ-Al_2O_3. These peaks can be associated with the reduction of the following species: nickel oxide weakly interacting with the γ-Al_2O_3 support (T < 550 °C), non-stoichiometric nickel aluminate species ($NiAl_xO_y$) between 550 and 750 °C and stoichiometric nickel aluminate species ($NiAl_2O_4$) at temperatures above 750 °C [1,43–48]. It should be noted that SGB method increased the proportion of species strongly interacting with the support favoring the nickel aluminates formation with high dispersion and making reduction more difficult [19–23].

The $PtNiAl^{(IWI)}$ catalyst showed a big hydrogen consumption peak at 320 °C, which can be assigned to the reduction of bulk nickel oxide or NiO species weakly interacting with the γ-Al_2O_3 support. This peak is 180 °C below the temperature reduction of similar species in the $NiAl^{(IWI)}$ catalyst. Thus it is associated with the Pt effect by hydrogen spillover phenomenon decreasing the temperature reduction required for nickel oxide. This can be directly

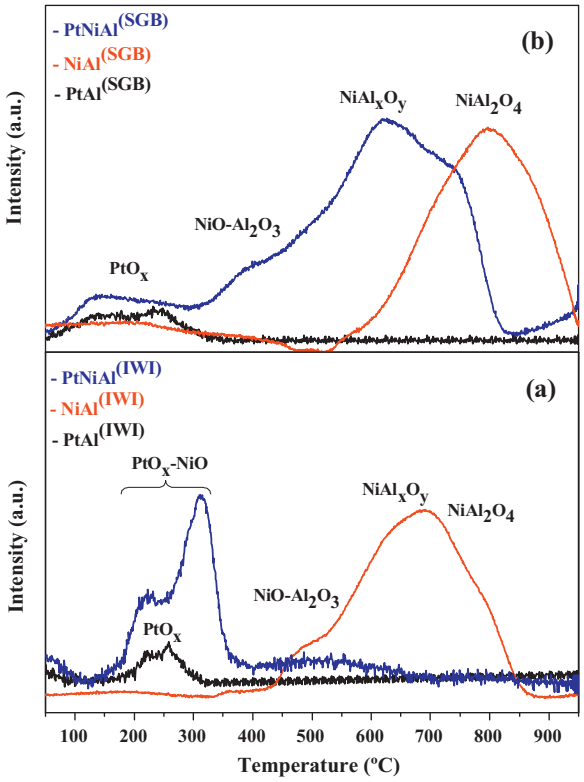

Fig. 3. Reducibility profiles obtained from TPR-H_2 analysis of Pt, Ni and PtNi catalysts, prepared by IWI (a) and SGB (b) methods.

Table 2
Average sizes of crystalline particles for calcined and reduced Pt, Ni and PtNi catalysts obtained by Scherrer equation from X-ray patterns.

Catalysts	d_{Pt^0/PtO_x}	d_{Pt^0}	$d_{NiO*/NiAl_xO_y**}$	d_{Ni^0}	$d_{\gamma\text{-}Al_2O_3}$	$d_{\gamma\text{-}Al_2O_3}$
	Calcined	Reduced	Calcined	Reduced	Calcined	Reduced
$PtAl^{(IWI)}$	7	13	–	–	5	5
$PtAl^{(SGB)}$	15	15	–	–	3	3
$NiAl^{(IWI)}$	–	–	7*	15	5	6
$NiAl^{(SGB)}$	–	–	2**	12	2	3
$PtNiAl^{(IWI)}$	12	15	19*	16	5	5
$PtNiAl^{(SGB)}$	5	5	3**	6	2	4

The unit of crystalline particles sizes is (nm).
* Correspond to NiO species.
** Correspond to $NiAl_xO_y$ species; $x, y \rightarrow$ index are between $0 \leq x \leq 2$ and $0 \leq y \leq 4$.

related to the dissociation of H_2 to $H^{\bullet}$ on Pt that penetrated into alumina and reduced more nickel at lower temperatures [44]. It is interesting to note that for the $PtNiAl^{(IWI)}$ catalyst, the NiO peak overlaps with PtO_x suggesting a possible interaction between these two components (PtO_x–NiO). This could facilitate the formation of PtNi alloys after reduction treatments with possible synergistic effects associated with electron transfers between the two metals phases [31]. It is also important to note that the Pt addition caused an important decrease in the nickel aluminate formation in this catalyst. At temperatures (above 350 °C the TPR-H_2 profile of $PtNiAl^{(SGB)}$ showed three reduction peaks that could be assigned to NiO-Al_2O_3, $NiAl_xO_y$ and $NiAl_2O_4$ species detected at the following temperature intervals: 370–490 °C, 490–620 °C and at above 730 °C, respectively. It should be noted that the reduction profile of SGB samples also showed a broad peak at higher temperatures when compared to their counterpart catalysts prepared by IWI. This observation can be explained as due to the higher interaction between active metals and support when sol–gel preparation procedure was used. This also generated a higher dispersion of Ni [19–23]. It is remarkable that the combination of Pt with Ni in bimetallic PtNi catalysts led to a cooperative effect between the two metal phases. On one side, Pt favored the reduction of $NiAl_xO_y$ at lower temperatures than the ones required for its counterpart Ni monometallic sample. On the other hand, it is interesting to observe that the $PtNiAl^{(SGB)}$ catalyst presented a broader and undefined peak of PtO_x reduction as compared to the equivalent $PtAl^{(SGB)}$ peak. This observation suggests that, probably, the co-incorporation of Ni and Pt by SGB method and a strong Ni–O–Al interaction caused by this methodology improved the Pt dispersion.

3.3. XRD characterization of catalysts

To identify and evaluate the degree of crystallinity and the reduction treatment effect over the catalysts prepared X-ray analysis of calcined and in situ reduced catalysts was used. The XRD patterns of Pt, Ni and PtNi-based γ-Al_2O_3 catalysts at calcined and reduced state are presented in Fig. 4.

Firstly, it is interesting to observe that the XRD patterns of calcined catalysts prepared by SGB presented a broad peak with lower intensity as compared to the IWI catalysts. This indicates that the elements of these catalysts are well dispersed showing an almost amorphous structure or poorly crystalline. This observation is in agreement with the high interaction demonstrated by TPR-H_2 analysis and the high surface areas exhibited by these samples. The XRD patterns of IWI catalysts showed lower dispersions indicating that these catalysts have a semi-crystalline structure. It can be noticed that all catalyst supports presented the characteristic features of a γ-Al_2O_3 (JCPDS 75-0921). Additionally, the diffractions peaks of SGB catalysts associated with γ-Al_2O_3 in the Ni-containing catalysts were broader peaks and showed a shift to a lower Bragg angle, suggesting a mixture of γ-Al_2O_3, $NiAl_xO_y$ and $NiAl_2O_4$ (JCPDS 01-1299) phases. This fact could be due to the high Ni–O–Al interaction, which led to a good dispersion of nickel species in the catalyst. Peaks related to NiO oxide were not detected.

In contrast, for the Ni-containing IWI catalysts the most intense reflections corresponding to NiO (JCPDS 65-6920) are clearly visible. While the nickel aluminate spinel structure was not detected, indicating that if these species were present, they would be quite small (below 2 nm) or their structure is nearly amorphous. These observations were in agreement with the results obtained from TPR-H_2 technique as commented above. In all catalysts, signals due to Pt metallic or PtO_x were detected, but it was not possible to differentiate among them [49–51].

After the reduction treatment, the crystallinity of Pt, Ni and PtNi catalysts was significantly increased as it can be observed in the reflections of the corresponding species, but the catalysts prepared by SGB always showed more dispersed phases than the IWI ones.

Regarding the patterns of reduced Ni-containing catalysts, it can be observed that reflections corresponding to NiO and $NiAl_2O_4$ phases disappeared and that new diffraction lines at 44° (1 1 1), 51.6° (2 0 0) and 75.6 (2 2 0) were detected. These diffraction angles are characteristics of a Ni metallic phase (JCDPS 04-850). In Pt-containing catalysts small diffractions lines were detected at 39.8° (1 1 1), 46.5° (2 0 0) and 67.8° (2 2 0). These lines can be attributed to a Pt metallic phase (JCPDS 01-1190) [1,9,32].

To evaluate the effect of the preparation method and the reduction treatment on the particles sizes just before catalytic activity tests, the average particle sizes of crystalline phases Pt^0/PtO_x, $NiO/NiAl_xO_y$, Ni^0 and γ-Al_2O_3 were estimated from XRD patterns of calcined and in situ reduced catalysts using Scherrer equation (7). The most intense reflections 43.16°/43.18° were used to estimate the sizes of $NiO/NiAl_xO_y$ phases, 44.5° for Ni, 39.8° for Pt/PtO_x and 65°–67.5° for γ-Al_2O_3. In fact, in order to carry out a good estimation of the particle sizes, a careful deconvolution of overlapping peaks was calculated. The estimated results are reported in Table 2.

For the calcined $PtNiAl^{(SGB)}$ catalysts, it can be realized that using the SGB method smaller particles of Pt^0/PtO_x were achieved as compared to the ones estimated for $PtAl^{(SGB)}$. This suggests that the co-incorporation of two metals (Pt, Ni) by SGB method favored their dispersion into all the catalyst matrix due to the higher interaction caused by SGB method. In the case of calcined $PtNiAl^{(IWI)}$ catalyst, the particles of Pt^0/PtO_x or NiO were considerably bigger than those estimated from data corresponding to the Pt or Ni monometallic catalysts counterparts. This suggests that the introduction of two metals (Pt, Ni) by IWI method hinders their dispersion on the support. This may be because the co-impregnation at the same time of Pt and Ni elements forced them to compete for the same surface causing their sintering.

The very good Ni species dispersion in SGB catalysts can be also attributed to the strong Ni–O–Al interaction produced by sol–gel and as a result small particles of nickel-aluminate spinels were

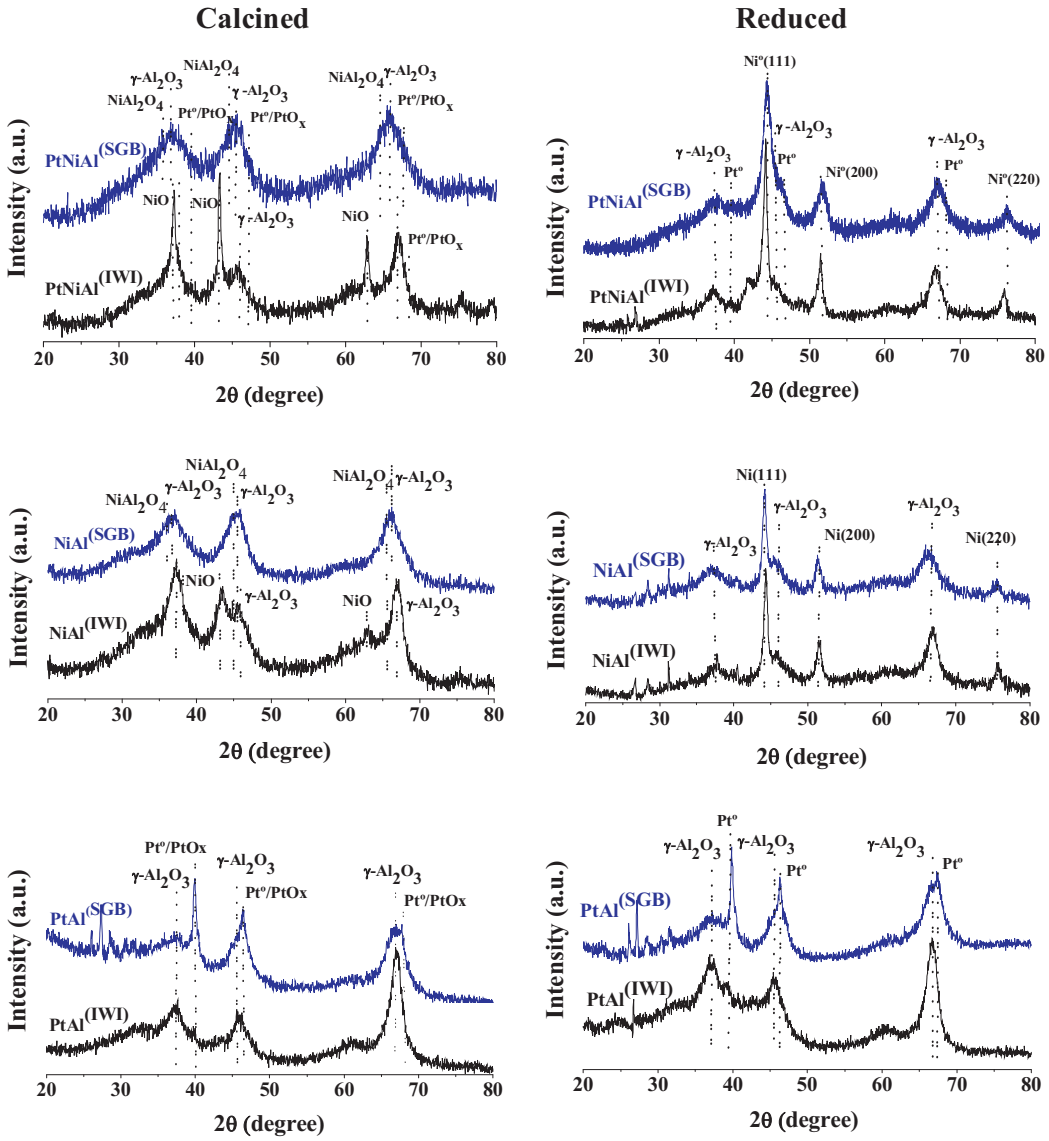

Fig. 4. X-ray patterns of calcined and in situ reduced Pt, Ni and PtNi catalysts prepared by IWI (black) and SGB (blue). (For interpretation of the references to color in this figure legend, the reader is referred to the web version of the article.)

generated [19–22]. PtNiAl$^{(SGB)}$ catalyst showed smaller particles related to Ni species (3 nm), particularly in the form of $NiAl_xO_y$ and $NiAl_2O_4$, than those detected in the PtNiAl$^{(IWI)}$ catalyst as NiO (20 nm). This indicates that the SGB method used promoted finer Ni particles formation [19–22].

After the reduction treatment of Pt-containing samples, the Pt particle size was doubled in PtAl$^{(IWI)}$ and significantly increased in PtNiAl$^{(IWI)}$. But in the SGB catalysts, the average of Pt particles size did not change, indicating that this method is effective to yield stable Pt particles even at high reduction temperatures (750 °C). For Ni-containing catalysts, the Ni particle size was bigger. But the average particle size of Ni was much smaller in SGB catalysts than in the corresponding IWI one. In the PtNiAl$^{(IWI)}$ catalyst a 16 nm was achieved, while in their counterpart PtNiAl$^{(SGB)}$ catalyst it did not exceed 6 nm. These observations confirmed the effectiveness of the SGB procedure to generate stable platinum and nickel small and well dispersed particles even if the reduction temperature is high (750 °C). It is also worth mentioning that the co-incorporation of Pt and Ni by SGB led to catalysts showing high active phases dispersion that showed strong resistance to sintering of platinum and nickel dispersed phases [19–22].

After the reduction treatment, the γ-Al_2O_3 particle diameter did not significantly change; probably because the reduction conditions used were soft. This suggests that this treatment did not alter the surface area and porosity of the catalysts, since that the γ-Al_2O_3 is the major component in all catalysts.

3.4. XPS characterization of catalysts

Calcined and in situ reduced Pt, Ni and PtNi catalysts were analyzed by XPS, in order to identify the dispersion and chemical state (oxidic or metallic) of elements which are present on the catalysts surface. Quantitative and qualitative XPS analyses are powerful tools in the interpretation of the surface composition and examine any change in the catalytic properties of catalysts after reduction treatment and as function to the method of preparation.

First, a known problem in the XPS study of Pt-containing catalysts must be considered. The Al2p line of γ-Al_2O_3 overlaps with the Pt4f line. Therefore, in this study Pt4d was used instead of Pt4f. This line is weaker but it is not overlapped by the spectral lines of the other components. The XPS spectra of $Pt4d_{5/2}$, $Ni2p_{3/2}$ core-levels with the corresponding deconvolutions are presented

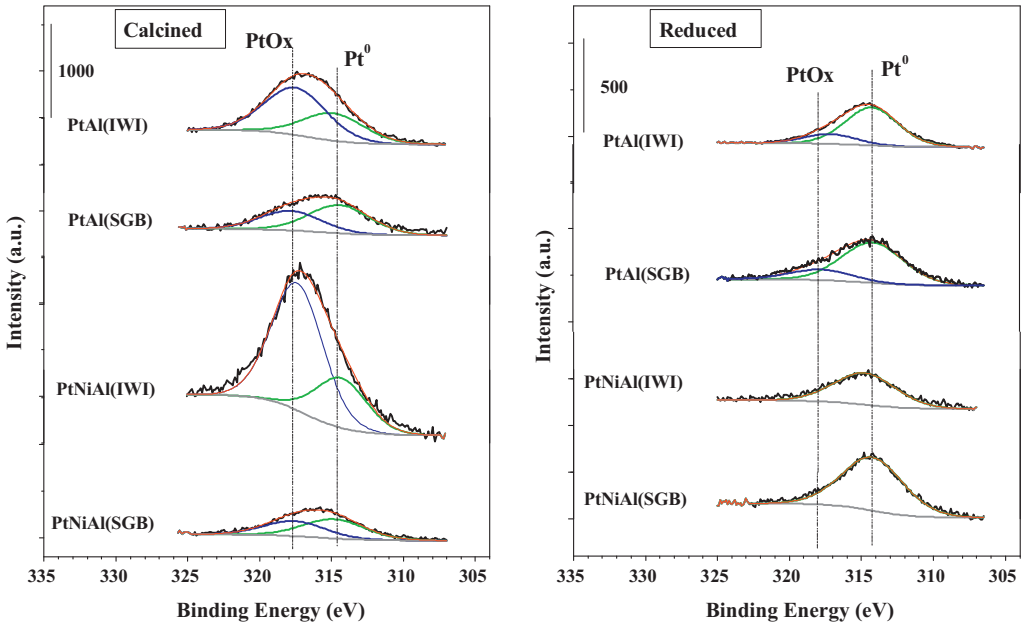

Fig. 5. XPS spectra of $Pt4d_{5/2}$ core-level for calcined and in situ reduced Pt-containing catalysts prepared by IWI and SGB methods.

in Figs. 5 and 6. The binding energies (BE) of these levels and the Ni/Al and Pt/Al atomic ratios for all calcined and reduced catalysts are summarized in Table 3.

For all the calcined and reduced catalysts, an Al2p level binding energy was measured at around 74.5 ± 0.5 eV. This energy is typically ascribed to Al^{+3} of γ-Al_2O_3 species.

The spectra of $Pt4d_{5/2}$ level for Pt-containing calcined catalysts are non-symmetrical, due to overlapping of signals related to different oxidation degrees of Pt. The Lorentzian/Gaussian deconvolution transforms it into two different signals. A first BE centered at 314.4–314.9 eV indicating the presence of Pt [49–52]. A second Pt BE observed at higher values 317.5–317.8 eV, corresponding to oxidized species of Pt, perhaps in the form of PtO_x [49–52]. The detection of PtO_x in these catalysts is in agreement with the XRD and TPR-H_2 results. These values are an intermediate value between 316 and 318 eV corresponding to the binding energy of PtO and PtO_2 [49–53]. This suggests that Pt showed an intermediate with δ+ charge. This charge could be related to broad peaks detected by TPR-H_2 for PtO_x species, which suggests that the platinum oxide phases having weakly and massif interactions with oxygen of γ-Al_2O_3.

After reduction treatment, the symmetry of the $Pt4d_{5/2}$ signal increased significantly. The Pt of bimetallic catalysts was reduced completely, while only part of the Pt (67–70%) was reduced in Pt monometallic catalysts. This indicates that the reduction of Pt

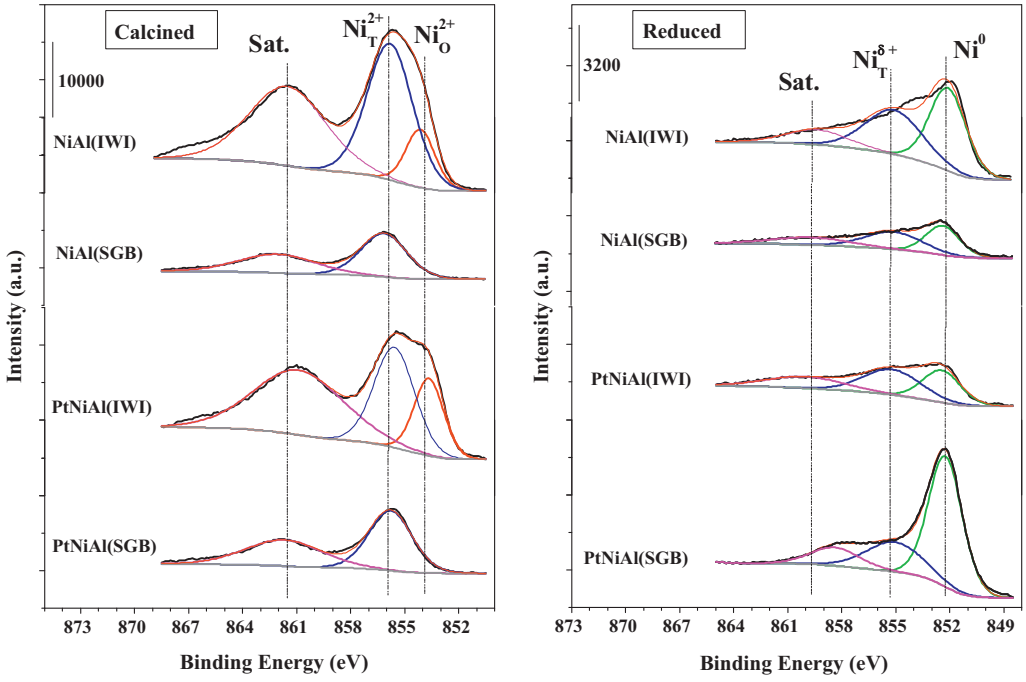

Fig. 6. XPS spectra of $Ni2p_{3/2}$ core-level for calcined and in situ reduced Ni-containing catalysts prepared by IWI and SGB methods.

Table 3
BE and population of Pt or Ni species in different oxidation states as well as atomic ratios for calcined and reduced Pt, Ni and PtNi catalysts.

Pt catalysts	B.E. Pt $4d_{5/2}$ (eV)			Ni catalysts	B.E. Ni $2p_{3/2}$ (eV)		
		Calcined	Reduced			Calcined	Reduced
$PtAl^{(IWI)}$	Pt^0	314.9 (37)	314.2 (67)	$NiAl^{(IWI)}$	Ni^0	–	852.1 (55)
	PtO_x	317.6 (63)	317.3 (33)		$Ni_O{}^{2+}$	854.1 (22)	–
					$Ni_T{}^{2+}$	855.8 (78)	855.1 (45)
	Pt/Al	0.019[a]	0.016[a]		Ni/Al	1.185[a]	0.119[a]
		0.009[b]				0.088[b]	
$PtAl^{(SGB)}$	Pt^0	314.4 (60)	314.2 (80)	$NiAl^{(SGB)}$	Ni^0	–	852.3 (48)
	PtO_x	317.8 (40)	317.7 (20)		$Ni_O{}^{2+}$	–	–
					$Ni_T{}^{2+}$	856.1 (100)	855.1 (52)
	Pt/Al	0.009[a]	0.009[a]		Ni/Al	0.171[a]	0.021[a]
		0.006[b]				0.077[b]	
$PtNiAl^{(IWI)}$	Pt^0	314.4 (28)	314.8 (100)	$PtNiAl^{(IWI)}$	Ni^0	–	852.4(44)
	PtO_x	317.4 (72)	–		$Ni_O{}^{2+}$	853.7 (36)	–
					$Ni_T{}^{2+}$	855.6 (64)	855.2 (56)
	Pt/Al	0.084[a]	0.014[a]		Ni/Al	0.992[a]	0.121[a]
		0.009[b]				0.098[b]	
$PtNiAl^{(SGB)}$	Pt	314.8 (57)	314.2 (100)	$PtNiAl^{(SGB)}$	Ni	–	852.2 (74)
	PtO_x	317.6 (43)	–		$Ni_O{}^{2+}$	–	–
					$Ni_T{}^{2+}$	856.4 (100)	855.1 (26)
	Pt/Al	0.012[a]	0.009[a]		Ni/Al	0.235[a]	0.088[a]
		0.008[b]				0.130[b]	

( ) → is population of different species.
a,b → atomic ratio calculated from XPS and ICP data, respectively.

monometallic catalysts at 350 °C was not enough to reduce the entire Pt.

The BE of $Pt4d_{5/2}$ core level (314.8 eV) for reduced PtNi catalysts prepared by IWI was slightly higher than its counterpart Pt monometallic catalyst (314.2 eV). Abu Bakar et al. [54–56] assigned this increase to the formation of metallic bands Pt–Ni or alloying of these metals. Probably, a part of Ni was incorporated into Pt structure changing its electronic environment via electron transfer between both elements. These crystallites were not detected by XRD, probably due to its nano-size (less than 2 nm). But this hypothesis also relies on TPR-H_2 results (see overlap between PtO_x and NiO bands reduction in Fig. 3(a)).

Regarding the binding energy of Pt^0, it is interesting to notice that the BE (314.8 eV) in the calcined $PtNiAl^{(SGB)}$ and $PtAl^{(IWI)}$ catalysts are higher (≈0.6 eV) than the BE of completely reduced Pt^0 (314.2 eV) in the same reduced catalysts. This means that the surface of Pt^0 particles tends to maintain some $\delta+$ charge; this can be related to the high Pt dispersion achieved on these catalysts. This observation is in agreement with the fine particle size estimated by XRD technique (see Table 2).

For calcined Ni monometallic catalysts, the $Ni2p_{3/2}$ core level spectra indicated that the Ni appeared in various states. It can be seen that two binding energies values for the Ni species were detected: one registered at 853.7–854.1 eV related to Ni^{2+} with pseudo octahedral coordination ($Ni_O{}^{2+}$), which is from NiO weakly interacting with γ-Al_2O_3 support. Another one at 855.8–856.4 eV, that can be associated with the presence of Ni^{2+} with pseudo tetrahedral coordination ($Ni_T{}^{2+}$), which is from $NiAl_xO_y$ and $NiAl_2O_4$ spinel structures [49–51]. It should be noticed that the signal corresponding to the NiO oxide was not detected in the catalysts prepared by SGB method. This result was attributed to a strong interaction of nickel with the γ-Al_2O_3 caused by sol–gel method. The sol–gel catalysts presented higher proportions of $Ni_T{}^{2+}$ (see Table 3) compared to impregnated catalysts. This high population of $Ni_T{}^{2+}$ confirmed the better Ni dispersion achieved using the SGB method [50,51].

For reduced Ni-containing catalysts, the $Ni2p_{3/2}$ core level showed a major peak in the range 851.1–852.4 eV, characteristic of Ni^0 [49]. The observation of the satellite line confirmed the presence of nickel ions surrounded with an oxygen environment. This satellite detection, together with the appearance of a second component of $Ni2p_{3/2}$ at 855.1–855.2 eV related to nickel ions strongly interacting with γ-Al_2O_3 lattice oxygen [49–51]. This species can be related to the presence of some Ni species not easily reduced. The values of BE were lower (≈0.8 eV) than the ones observed for the counterpart calcined catalysts. This fact suggests that the superficial Ni ions had some oxygen deficit.

The amount of reduced nickel in the Ni monometallic catalysts decreased slightly following this order: $NiAl^{(IWI)} > NiAl^{(SGB)}$. This can be explained through the high interaction induced by SGB method well demonstrated by TPR-H_2 and XRD results, since that the Ni highly interacted requires more temperature for its reduction. This amount was higher in the $PtNiAl^{(SGB)}$ catalyst if compared to its counterpart Ni catalyst and this can be related to H_2 spillover favored by the high Pt dispersion of this catalyst. The high proportion of $Ni_T{}^{2+}$ detected in the reduced $PtNiAl^{(IWI)}$ may be linked by one side, probably, to a segregation of fine $NiAl_2O_4$ particles (not reduced) on the surface of Ni^0 particles. Secondly, it can be related to the decoration phenomenon (deposition of Pt^0 over Ni^0) [1]. Nevertheless, the intensity of $Ni2p_{3/2}$ level (see Fig. 6) and Ni/Al atomic ratio (see Table 3) showed by calcined $PtNiAl^{(IWI)}$ was lower than the intensity of $Ni2p_{3/2}$ level and Ni/Al ratio of calcined $NiAl^{(IWI)}$. In addition, it can be observed an increase in $Pt4d_{5/2}$ intensity and Pt/Al atomic ratio for calcined $PtNiAl^{(IWI)}$ when compared to $PtAl^{(IWI)}$ catalyst. This observation indicates that probably part of the Ni surface was covered by Pt deposited during the impregnation of this catalyst.

The comparison of atomic ratios showed that the Pt/Al and Ni/Al surface ratios estimated by XPS for calcined IWI catalysts are higher than those of the bulk ratios calculated from ICP data. This indicates that Pt and Ni were preferentially deposited on the outer surface of γ-Al_2O_3. However, for SGB catalysts these atomic ratios were much more close to these bulk values, indicating that the metal loading of Ni and Pt was homogeneously distributed inside the catalyst matrix. In addition, the XPS atomic ratio of Ni/Al for Ni-containing catalysts decreased following the order IWI > SGB. However, the superficial $Ni_T{}^{2+}$ species on the SGB catalysts exhibit BE slightly

greater than those the IWI catalysts. This suggests that there was greater superficial interaction of Ni–O–Al in the SGB catalysts. This corroborates the well dispersion demonstrated by X-ray diffraction and TPR-H_2 analysis.

Comparing the Pt/Al ratio of Pt-containing reduced and calcined catalysts, the SGB catalyst presented similar Pt/Al ratios, while this ratio was lower in the reduced IWI catalyst than in the corresponding calcined one. This indicates that in the IWI catalysts Pt crystallites suffered sintering during reduction [54], while the SGB method showed to be very effective to inhibit the agglomeration of Pt particles; even if they were reduced at a high temperature (750 °C). As a result the Pt dispersion achieved through sol–gel preparation procedure was maintained. However, for Ni-containing catalysts the Ni/Al ratios decreased for all of them after being treated under reducing conditions if compared with their calcined counterparts. This suggested a possible sintering of surface Ni particles, as the literature [54] indicates. It could also have been due to the migration of metal species into the inner porous structure of the support. But this decrease in Ni/Al is less pronounced for SGB catalysts. These results are well corroborated by the results obtained by XRD and the high specific areas obtained for these catalysts.

3.5. APR tests of Pt or/and Ni catalysts

As described earlier, each prepared catalyst was tested at 250 °C/50 bar and 230 °C/30 bar in order to compare the influence of these operating conditions over the activity and stability of these catalysts. The glycerol conversions of all catalysts at steady state (30–32 h) are shown in Fig. 7 and Table 4. The best behaviors reached using the PtNi bimetallic catalysts are also presented in Fig. 8(a and b).

Analyzing Figs. 7 and 8(a and b) and Table 4, it can be observed that the glycerol conversions obtained were related to its transformation into gaseous products and intermediate OHCs. At steady state, the major gaseous products formed in the activity tests were mainly H_2, CO_2, CH_4 and small amounts of C_2H_6 and C_3H_8. Traces of CO (<50 ppm) were detected because APR occurred at high total pressure and high water partial pressure. The adsorbed CO species reacted with water via WGS reaction (4) to form CO_2 and H_2. It has been reported [8–10] that the gas bubbles formed within the liquid phase contain water vapor at a pressure equal to its saturation pressure at the reactor temperature, favoring the WGS reaction and leading to very low CO concentrations. On the other hand, in liquid phase, OHCs were detected and measured such as C_1 (methanol), C_2 (acetic acid, acetaldehyde, ethylene glycol) and C_3 (2-propanol, acetol, 1,2-propanediol).

Operating at 250 °C/50 bar, the catalysts activity (glycerol conversions; conversions into gas) followed this order (see Fig. 7): $PtNiAl^{(SGB)}$(73%;27%) > $PtNiAl^{(IWI)}$(65%;17%), $NiAl^{(SGB)}$(40%;9.5%) > $NiAl^{(IWI)}$(10%;1.1%). For the Pt monometallic catalysts, the opposite order for glycerol conversion was found: $PtAl^{(IWI)}$(31%) > $PtAl^{(SGB)}$(19.3%). Nevertheless the same order for conversion into gas was maintained: $PtAl^{(SGB)}$(6.5%) > $PtAl^{(IWI)}$(4.5%). At 230 °C/30 bar similar results were measured, the conversions presented the following order: $PtNiAl^{(SGB)}$(75%; 28%) > $PtNiAl^{(IWI)}$(35%; 6%), $NiAl^{(SGB)}$(19%; 5.3%) > $NiAl^{(IWI)}$(4%; 0.8%). In the case of Pt monometallic ones, the order was $PtAl^{(IWI)}$(17.3%) > $PtAl^{(SGB)}$(13.2%) for glycerol conversion and $PtAl^{(SGB)}$(5%) > $PtAl^{(IWI)}$(4%) for conversion into gas. These conversions at 230 °C/30 bar were slightly lower than those at 250 °C/50 bar, but the behavior of the catalysts was more stable at these less severe conditions (see Fig. 8(a and b)).

Comparing the catalytic activity of all catalysts at both conditions, it can be observed that the PtNi bimetallic catalysts exhibited higher conversions than the sum of the conversions achieved by the corresponding monometallic Pt and Ni catalysts. This confirmed the promoting cooperative effect between Pt and Ni in the bimetallic catalysts. The oxygenated molecule is decomposed on Pt/or Ni by dehydrogenation, followed by C—C cleavage (3) to give H_2 and adsorbed CO which is converted immediately to CO_2 by WGS [9]. The cooperative effect is well corroborated by the possible existence of PtNi alloy in the $PtNiAl^{(IWI)}$ catalyst (TPR-H_2, XPS), by the clear enhancement of Pt and Ni species dispersion in bulk and at the surface caused by Ni co-combination in the $PtNiAl^{(SGB)}$ catalyst (XRD, XPS), and by the H_2 spillover which favored the reduction of more amounts of Ni at low temperature (TPR-H_2).

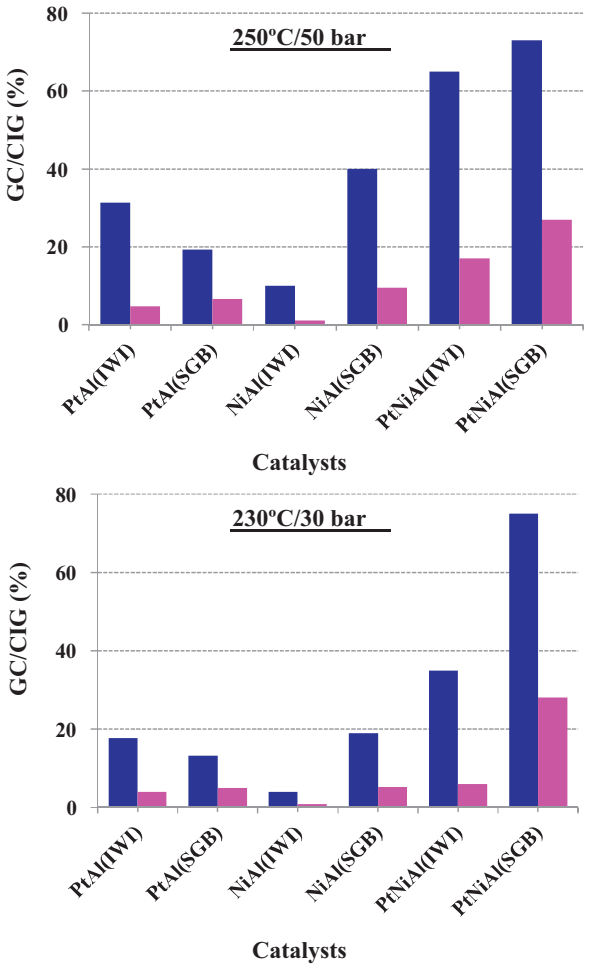

Fig. 7. Glycerol conversion (blue) and conversion into gas (magenta) obtained by APR of 10 wt% $C_3H_8O_3/H_2O$ mixture on Pt, Ni and PtNi catalysts at 250 °C/50 bar and 230 °C/30 bar (1 g of catalysts, feed rate of 0.4 mL/min, WHSV = 2.6 h^{-1}, steady state 30–32 h). (For interpretation of the references to color in this figure legend, the reader is referred to the web version of the article.)

It is interesting to note that all SGB catalysts presented higher conversions, especially in the case of conversion into gas, than the IWI catalysts. This observation indicates that these catalysts were more able to convert the glycerol and the intermediate products into gaseous products. This could be due to better surface properties achieved by sol–gel method. SGB catalysts showed high surface area and porosity (Table 1) facilitating the adsorption of intermediate molecules and rising the contact time with Pt and/or Ni particles highly dispersed and converting them into gaseous products.

The catalysts prepared by SGB method generated higher gas flows than their counterparts prepared by IWI (Table 4). This can be explained by a higher capacity of these catalysts to reform the OHCs into gaseous products. This difference was more pronounced at moderate temperature/pressure conditions; 230 °C/30 bar (see

Table 4
Catalytic performance for APR of 10 wt% glycerol/water mixture on the Pt, Ni and PtNi catalysts at 250 °C/50 bar and 230 °C/30 bar (1 g of catalysts, feed of 0.4 mL/min, WHSV = 2.60 h^{-1}, steady state 30–32 h).

Catalyst	T(°C)/P(bar)	F_T	Selectivity (%)		H_2/CO_2	Yield_OHCs (j)		
			H_2	Alkanes		C_1	C_2	C_3
$PtAl^{(IWI)}$	250/50	3.2	61	17	60/36	–	0.02	0.15
	230/30	3.9	84	18	67/28	–	0.01	0.08
$PtAl^{(SGB)}$	250/50	6.1	91	5	69/30	0.01	0.01	0.06
	230/30	6.5	90	15	69/27	–	0.04	0.05
$NiAl^{(IWI)}$	250/50	0.4	16	35	27/49	–	–	0.05
	230/30	0.6	34	13	46/50	–	–	0.01
$NiAl^{(SGB)}$	250/50	3.5	13	51	23/39	–	0.03	0.24
	230/30	2.0	15	40	27/46	–	0.01	0.14
$PtNiAl^{(IWI)}$	250/50	11.0	42	27	50/37	0.02	0.10	0.27
	230/30	3.5	38	17	47/45	–	0.03	0.16
$PtNiAl^{(SGB)}$	250/50	14.5	27	38	39/38	0.02	0.09	0.24
	230/30	19.5	50	21	54/37	0.04	0.16	0.20

F_T → Flow of total gas formation (mL (STP) min^{-1} $g_{cat.}{}^{-1}$).
H_2/CO_2 → molar ratio.
Yield_OHCs (j) → yield of C_1 (methanol), C_2 (acetic acid, acetaldehyde, ethylene glycol) and C_3 (2-propanol, acetol, 1,2-propanediol, excluding unconverted glycerol).

Fig. 8(a and b)). The Pt catalysts promoted gas flows with higher H_2 selectivity, while the Ni counterparts were more selective to alkanes formation. The PtNi catalysts presented an intermediate behavior: moderate H_2 and alkanes selectivity. On the one hand, the better H_2 selectivity obtained by Pt catalysts is due to the high activity of this element for dehydrogenation reactions (C—H cleavage) [4–10]. In fact, the APR reaction generated H_2 and CO_2 composition very close to the stoichiometric values; H_2/CO_2 (≈2.4)

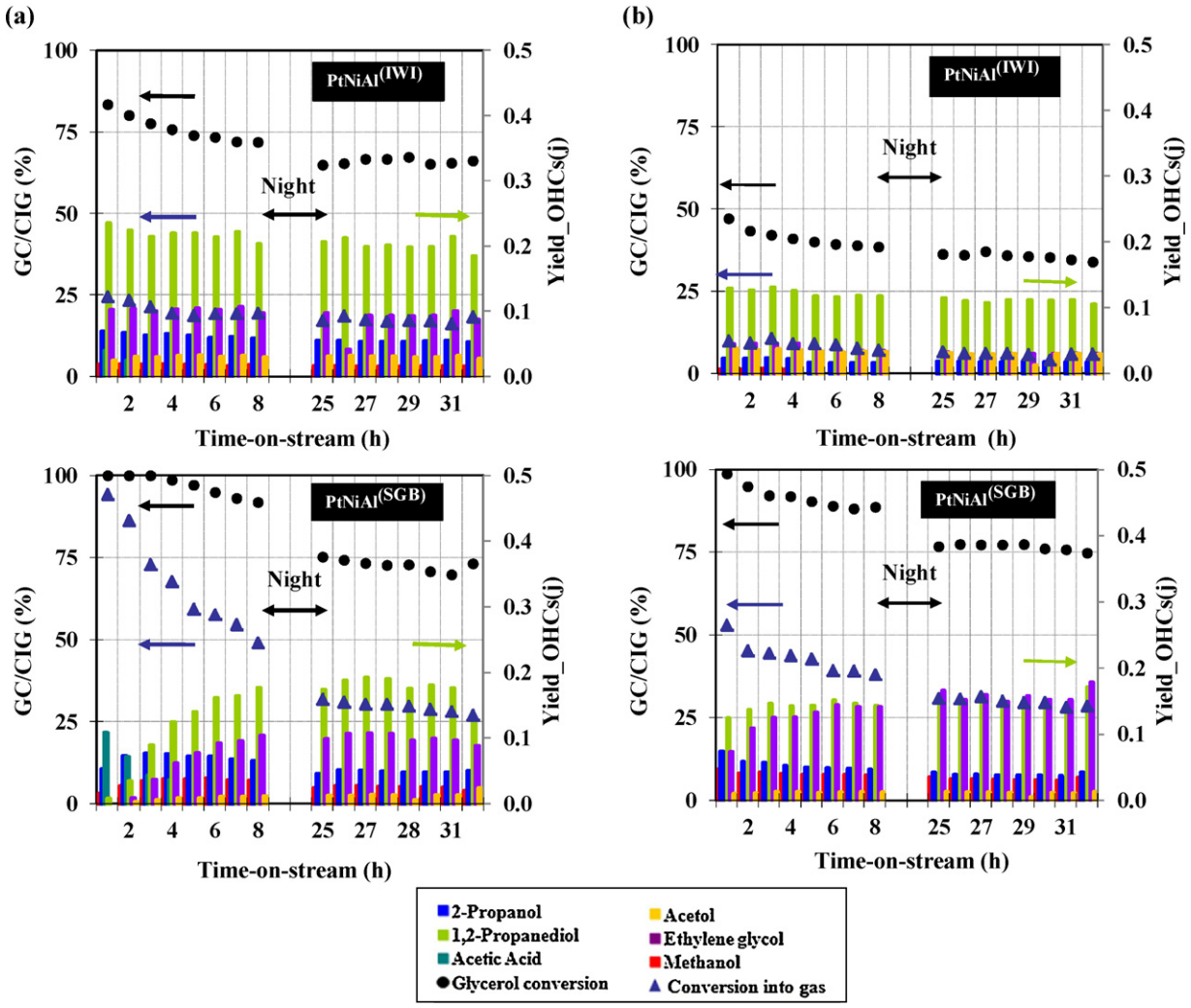

Fig. 8. (a) Glycerol conversion and conversion into gas, as well as yield distribution of OHCs as a function of time-on-stream for APR of 10 wt% $C_3H_8O_3/H_2O$ mixture on PtNi bimetallic catalysts at 250 °C/50 bar (1 g of catalysts, feed rate of 0.4 mL/min, WHSV = 2.6 h^{-1}). (b) Glycerol conversion and conversion into gas, as well as yield distribution of OHCs as a function of time-on-stream for APR of 10 wt% $C_3H_8O_3/H_2O$ mixture on PtNi bimetallic catalysts at 230 °C/30 bar (1 g of catalysts, feed rate of 0.4 mL/min, WHSV = 2.6 h^{-1}).

ratios achieved are near to its theoretical value (2.33). On the other hand, the high selectivity to alkanes formed when Ni catalysts were used can be related to the high activity of Ni for the hydrogenation of CO/CO_2 reactions and for the cleavage of C—C/C—O bonds of oxygenated compounds via consecutive and/or parallel reactions [4–10]. This second explanation is more probable since very low molar H_2/CO_2 ratios were obtained (27/49–46/50) as compared to the theoretical value (70/30). The excess of CO_2 generated suggests that the alkanes were formed directly from OHCs. The moderate selectivity values of H_2 and alkanes when PtNi catalysts were used are due to the above mentioned cooperative effect between both metals. This effect was more pronounced for the $PtNiAl^{(SGB)}$ catalyst. In this case it is more probable that some light alkanes were formed from CO_2 via methanation and Fischer–Tropsch reaction. This can be related to the increment of H_2/CO_2 ratios (39/38–54/36) associated with the diminution of CO_2 proportion in the product gases (near the stoichiometric value, 30%). Therefore, one of the keys of glycerol conversion by APR process is to improve these catalysts to be more selective toward H_2 formation. For this it is necessary to lower their activities to catalyze methanation and Fischer–Tropsch reactions and to increase their activities to reform all the intermediate products initially generated from glycerol under APR conditions.

The data presented in Table 4 shows that the APR process promoted more H_2 formation at 230 °C/30 bar than at 250 °C/50 bar. This suggests that operating at relatively moderate temperatures/pressures is much more selective to H_2 formation by APR of glycerol. This can be related, probably, to the effect of pressure, since lower pressures favor the formation of compounds through reaction increasing the total number of gaseous moles (as $7H_2$ according to Eq. (2)) increasing thus the total gas flow formed (see Table 4).

Comparing the distribution of OHCs in the liquid phase (Table 4), it can be observed that SGB Pt-containing catalysts increased relatively the yields of oxygenated C_1 and C_2 compounds such as methanol, acetic acid, ethylene glycol, against the C_3 compounds formation (2-propanol, acetol, 1,2-propanediol) as compared with their counterparts IWI catalysts. This result is more pronounced at 230 °C/30 bar conditions. This was a consequence of the competition enhancement of the C—C/C—H against the C—O bonds cleavage over these catalysts. Therefore, the APR process on these catalysts led to a more gas (Table 4), since as it has been reported above this is in agreement with its higher activity for C—C/C—H bond breaking, WGS reaction and methanation/Fischer–Tropsch reactions.

After several hours on stream, the glycerol conversion and gaseous products formation decreased gradually (Fig. 8(a and b)). This trend was simultaneously accompanied with significant increases in OHCs formation (particularly C_3) until the catalysts reached their steady state. According to the literature [8–10,29], these liquid products are formed by dehydration/hydrogenation reactions. This confirmed that the hydrogenolysis and/or cleavage of the C—O bonds mainly occurred on catalysts explaining the decrease in the conversion into gas at steady state. It should be noted that in the first hours of reaction, the APR of glycerol, particularly over $PtNiAl^{(SGB)}$ catalysts, produced slightly more alcohols (methanol, 2-propanol) and acids (acetic acid) as intermediates in liquid phase, when the process was much more selective to the formation of light gaseous products. At steady state, the major OHCs formed were 1,2-propanediol and ethylene glycol, and the conversion into gas was lower. This observation indicates that the mechanism of gaseous products formation during the first hours-on-stream was different to the mechanism when the system reached its steady state. This is probably due to the modification of the active sites on the catalysts surface. This was confirmed by XRD analysis of spent PtNi catalysts whose results are showed in Fig. 9(a). It can be seen that the XRD peaks indicate, especially for the $PtNiAl^{(SGB)}$ catalyst, that a part of γ-Al_2O_3 support was transformed into γ-AlOOH after the reaction. The surface hydroxyl groups of γ-AlOOH show higher acidity [2], and when these new sites start to intervene in the reaction they can modify the reaction mechanism.

However, the decrease in catalytic activity as a function of time-on-stream for PtNiAl (Fig. 8(a and b)) and NiAl catalysts (behavior not represented) suggests that the Ni-containing catalysts were subjected to deactivation, resulting in a loss of the activity for C—C/C—H breaking bonds thus increasing the OHCs formation via C—O cleavage/dehydration reaction on the support. The deactivation of the Ni species was also observed by Wen et al. [2], who found that the Ni atoms are highly susceptible to oxidation by water excess at low temperatures, since the oxidized Ni is inactive for the glycerol aqueous-phase reforming at low temperature. This suggestion was supported by the results obtained from the XPS analysis of spent PtNi catalysts presented in Fig. 9(b). The $Ni2p_{3/2}$ spectra showed that after APR reaction at 250 °C/50 bar, a higher proportion of Ni species was reoxidized (BE of 855.4–856.2 eV). In addition, the intensity of $Ni2p_{3/2}$ spectra decreased as compared to the as-reduced catalysts counterparts (see Figs. 6 and 9(b)) suggesting some sintering of Ni particles. The XRD patterns also showed narrower Ni lines, indicating that the sintering of Ni particles occurred during the APR reaction. According to the Scherrer equation (7), the crystallite size of Ni after reaction was 30 nm for SGB catalyst and 35 nm for IWI catalyst, which are larger than the values of 9 nm and 16 nm estimated for the as-reduced catalysts counterparts, respectively. All these observations confirmed that the active sites suffered quantitative and qualitative changes, which can be responsible of the deactivation of the Ni-containing catalysts.

3.6. General discussion

Finally, it should be noticed that the results obtained in this work using SGB catalysts are more promising than those obtained in previous works using similar PtNi-based catalysts [31], and than other results recently published [2,8–12,23–26,57–59] about APR of glycerol. This higher activity is more pronounced in what concerns conversion into gaseous products, the objective of this work. This represents an improvement on the subject of H_2 production from glycerol by aqueous phase reforming process.

This work proves that Pt or/and Ni catalysts prepared by SGB method, especially bimetallic catalysts, are intrinsically more active than their equivalent impregnated catalysts. Their higher activities can be explained as due to better catalytic properties achieved by SGB method in terms of surface area, porosity, finer size of Pt and Ni particles and cooperative effect between these two elements.

In general, the SGB catalysts showed higher activity to convert glycerol into gas, while the IWI catalysts were more selective to the formation of intermediate OHCs. The $PtNiAl^{(SGB)}$ and $PtNiAl^{(IWI)}$ bimetallic catalysts achieved higher glycerol conversions than their Pt or Ni counterparts. This suggests that the Ni combination with Pt has an important promotional effect on the glycerol conversion. This improvement may be due, among other reasons, to the increase in active sites due to their higher experimental loading (10–12 wt%) and to the enhancement of Ni reducibility by Pt-spillover, especially for Ni-spinels of $PtNiAl^{(SGB)}$ catalyst, since these highly dispersed crystallites provide the contact time for glycerol/OHCs being reformed to gaseous products.

In the same context, it should be noticed that when catalysts were fresh and reduced, particularly in the case of the SGB catalysts, the glycerol conversion seems to be controlled by C—C/C—H rather than C—C/C—O cleavage favoring more gas formation and less OHCs products as C_1 and C_2 (see Fig. 8a and b). These bond breakings happened on the surface of metals and thus the attempts to rationalize the mechanism of aqueous-phase reforming of

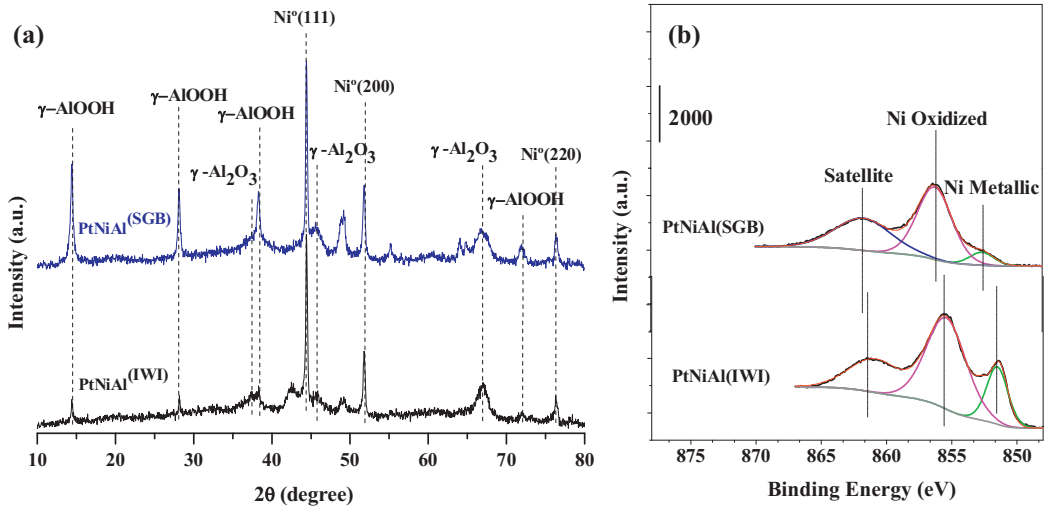

Fig. 9. X-ray patterns (a) and XPS spectra of $Ni2p_{3/2}$ core-level (b) for PtNi-bimetallic catalysts after reaction at 250 °C/50 bar (IWI (black) and SGB (blue)). (For interpretation of the references to color in this figure legend, the reader is referred to the web version of the article.)

oxygenated hydrocarbons presented so far in the literature rely almost exclusively on the metallic centers [8–12]. However at steady state, the APR of glycerol is favored by dehydration/hydrogenation reactions and C—C and C—O bonds cleavage favoring more formation of OHCs as 1,2-propanediol, ethylene glycol and acetol. These products detected in the liquid product stream were typically obtained from C—C and C—O bonds hydrogenolysis [8–10,29,31]. This suggests that a possible role played by the γ-Al_2O_3 should not be ruled out completely as already previously suggested by Shabaker et al. [60] in their studies carried out with ethylene glycol. This also indicates that these catalysts take this pathway because of probable modifications of the active centers or due to deactivation processes suffered during the reaction. Therefore, γ-Al_2O_3, particularly those of high surface area prepared by SGB method, as the one employed in this APR study can contribute directly to increase the conversion of glycerol and/or play a key role in selectivity.

4. Conclusions

The Pt or/and Ni-based γ-Al_2O_3 catalysts were prepared by two methods for comparative purposes and studied using a variety of physicochemical methods. All systems were tested in the APR of glycerol to H_2 production. The most important findings of the present study may be summarized as follows:

The catalytic properties of Pt or/and Ni-based γ-Al_2O_3 catalysts are considerably affected by the method of preparation. The basic agent used in the SGB method generated an increase in condensation reactions and led to clusters characterized by a spherical shape. This method generated spinel-type catalysts having very high surface area, which is not achieved when these catalysts are prepared by IWI method. The SBG methodology is able to ensure a better compromise between Pt–Ni dispersions and interactions and led to catalysts with higher capacity to inhibit particles sintering during the reduction treatment. This method is very promising to prepare Pt-Ni catalysts for glycerol transformation into gaseous products by APR process.

The activity tests also confirmed that the activity and stability of the catalysts were significantly affected by the preparation method and the nature of active sites. The SGB catalysts showed to be more active, while the equivalent IWI catalysts are more stable, especially operating at moderate temperatures/pressures. The higher activity exhibited by SGB catalysts compared to IWI catalysts counterparts may be due to better catalytic properties achieved by SGB method in terms of surface area, porosity, dispersion, and resistance against sintering of Pt or/and Ni particles during the reduction treatment and a possible cooperative effect between these two elements.

The $PtNiAl^{(SGB)}$ catalyst showed the best catalytic activity and stability. This catalyst was found to be extremely active for gaseous products formation through aqueous reforming of glycerol. This system proved to be also a good catalyst for WGS reactions, as CO was not significantly detected. The glycerol was mainly converted into gas phase by cracking of C—C/C—H bonds, dehydrogenation reactions, WGS, methanation/Fischer–Tropsch and to a lesser extent to intermediate OHCs by dehydration/hydrogenolysis reactions. These results confirmed that Pt combined with Ni and the formation of non-stoichiometric Ni spinels during preparation by SGB were crucial for $PtNiAl^{(SGB)}$ catalyst being able to maintain these two elements highly dispersed after the activation–reduction treatment.

Regarding the results obtained using Pt or Ni monometallic catalyst, it has been shown that Pt and Ni are active elements to catalyze APR of glycerol but Pt or Ni did not present enough activity for the conversion of glycerol into gaseous products when APR is used. The simplest method to achieve the required catalytic activity is to combine both metals using SGB method to obtain a better glycerol APR performance.

Acknowledgements

This work was carried out in the laboratory of the "Sustainable Process Engineering" research group (University of the Basque Country (UPV/EHU), Spain) in collaboration with the "UCCS" research unit (University of Science and Technology of Lille, France), supported by funds from the Spanish Ministry of Science and Innovation (Project: ENE2011-23950) and the Basque Regional Government. The authors gratefully acknowledge institutions for providing financial support, as well as express their gratitude to L. Burylo for XRD analysis and Dr. A. S. Mamede, M. Trentesaux and A. Beaurain for XPS analysis. The Fonds Européen de Développement

Régional (FEDER), CNRS, Région Nord Pas-de-Calais and Ministère de l'Education Nationale de l'Enseignement Supérieur et de la Recherche are acknowledged for fundings of XPS/LEIS/ToF-SIMS spectrometers within the Regional Platform of Surface Analysis.

References

[1] A. Iriondo, V.L. Barrio, J.F. Cambra, P.L. Arias, M.B. Güemez, R.M. Navarro, M.C. Sanchez-Sanchez, G.J.L. Fierro, Topics in Catalysis 49 (2008) 46–58.
[2] G. Wen, Y. Xu, H. Ma, Z. Xu, Z. Tian, International Journal of Hydrogen Energy 33 (2008) 6657–6666.
[3] G.W. Huber, S. Iborra, A. Corma, Chemical Reviews 9 (2006) 4044–4098.
[4] S. Adhikari, S.D. Fernando, A. Haryanto, Energy Conversion and Management 50 (2009) 2600–2604.
[5] P.D. Vaidya, A.E. Rodrigues, Chemical Engineering and Technology 32 (2009) 1463–1469.
[6] A. Haryanto, S. Fernando, N. Murali, S. Adhikari, Energy and Fuels 19 (2005) 2098–2106.
[7] N. Meng, Y.C.L. Dennis, K.H.L. Michael, International Journal of Hydrogen Energy 32 (2007) 3238–3247.
[8] R.R. Davda, J.W. Shabaker, G.W. Huber, R.D. Cortright, J.A. Dumesic, Applied Catalysis B: Environmental 56 (2005) 171–186.
[9] R.D. Cortright, R.R. Davda, J.A. Dumesic, Nature 418 (2002) 964–967.
[10] G.W. Huber, J.W. Shabaker, J.A. Dumesic, Science 300 (2003) 2075–2077.
[11] J.W. Shabaker, R.R. Davda, G.W. Huber, R.D. Cortright, J.A. Dumesic, Journal of Catalysis 215 (2003) 344–352.
[12] J.W. Shabaker, R.R. Davda, G.W. Huber, R.D. Cortright, J.A. Dumesic, Catalysis Letters 88 (2003) 1–8.
[13] I.O. Cruz, N.F.P. Ribeiro, D.A.G. Aranda, M.V.M. Souza, Catalysis Communications 9 (2008) 2606–2611.
[14] D. Wang, D. Montane, E. Chornet, Applied Catalysis A-General 143 (1996) 245.
[15] I. Gandarias, P.L. Arias, J. Requies, M. El Doukkali, M.B. Güemez, Journal of Catalysis 282 (2011) 237–247.
[16] A. Behr, J. Eilting, K. Irawadi, J. Leschinski, F. Lindner, Green Chemistry 10 (2008) 13–30.
[17] C.K. Lambert, R.D. Gonzalez, Materials Letters 38 (1999) 145–149.
[18] E. Díaz, S. Ordónez, A. Vega, J. Coca, Microporous and Mesoporous Materials 70 (2004) 109–118.
[19] A.L. Ahmad, N.N.N. Mustafa, International Journal of Hydrogen Energy 32 (2007) 2010–2021.
[20] I.H. Cho, S.B. Park, S.J. Cho, R. Ryoo, Journal of Catalysis 173 (1998) 295–303.
[21] L. Hu, K.A. Boateng, J.M. Hill, Journal of Molecular Catalysis A: Chemical 259 (2006) 51–60.
[22] A. Vazquer, T. Lopez, R. Gomez, Journal of Molecular Catalysis A: Chemical 167 (2001) 91–99.
[23] A. Tanksale, C.H. Zhou, J.N. Beltramini, G.Q. Lu, Journal of Inclusion Phenomena and Macrocyclic Chemistry 65 (2009) 83–88.
[24] F. Xie, X. Chu, H. Hu, M. Qiao, S. Yan, Y. Zhu, H. He, K. Fan, H. Li, B. Zong, X. Zhang, Journal of Catalysis 241 (2006) 211–220.
[25] R.R. Davda, J.W. Shabaker, G.W. Huber, R.D. Cortright, J.A. Dumesic, Applied Catalysis B: Environmental 43 (2003) 13–26.
[26] G.W. Huber, J.W. Shabaker, S.T. Evans, J.A. Dumesic, Applied Catalysis B: Environmental 62 (2006) 226–235.
[27] D.A. Simonetti, E. Kunkes, J.A. Dumesic, Journal of Catalysis 247 (2007) 298–306.
[28] N.J. Luo, X.W. Fu, F.H. Cao, P.P. Edwards, Fuel 87 (2008) 3483–3489.
[29] A. Wawrzetz, B. Peng, A. Hrabar, J.A. Lercher, Journal of Catalysis 269 (2010) 411–420.
[30] D.L. King, L. Zhang, G. Xia, M. Karim, D.J. Heldebrant, X. Wang, T. Peterson, Y. Wang, Applied Catalysis B: Environmental 99 (2010) 206–213.
[31] A. Iriondo, J.F. Cambra, V.L. Barrio, M.B. Guemez, P.L. Arias, M.C. Sanchez-Sanchez, R.M. Navarro, J.L.G. Fierro, Applied Catalysis B: Environmental 106 (2011) 83–93.
[32] M. El Doukkali, A. Iriondo, P.L. Arias, J.F. Cambra, I. Gandrias, V.L. Barrio, International Journal of Hydrogen Energy 37 (2012) 8298–8309.
[33] A. Iriondo, V.L. Barrio, M. El Doukkali, J.F. Cambra, M.B. Güemez, J. Requies, P.L. Arias, M.C. Sanchez-Sanchez, R.M. Navarro, J.L.G. Fierro, International Journal of Hydrogen Energy 37 (2012) 2028–2036.
[34] F. Dumeignil, K. Sato, M. Imamura, N. Matsubayashi, E. Payen, H. Shimada, Applied Catalysis A-General 241 (2003) 319–329.
[35] O.C., Gobin, Ph.D Thesis in Laval University, Ste-Foy-Canada, 2006.
[36] A. Carati, G. Ferraris, M. Guidotti, G. Moretti, R. Psaro, C. Rizzo, Catalysis Today 77 (2003) 315–323.
[37] S. Kondo, T. Ishikawa, I. Abe (Eds.), Kyuchaku no Kagaku, Maruzen, Tokyo, 1991.
[38] L. Xu, K. Chen, J. Zhu, H. Chen, H. Huang, J. Xu, X. Huang, Superlattices and Microstructures 29 (2001) 67–72.
[39] O. Wind, F. Gingele, U. Woggon, Journal of Luminescence 300 (1997) 72–74.
[40] C. Otero Arean, et al., Materials Letters 39 (1999) 22–27.
[41] A. Sirijaruphan, J.G. Goodwin, R.W. Rice, Journal of Catalysis 224 (2004) 304–413.
[42] D.O. Hayward, B.M.W. Trapnell, Chemisorption, second ed., Butterworths, London, 1964.
[43] G. Li, L. Hu, J.M. Hill, Applied Catalysis A-General 301 (2006) 16–24.
[44] A. Tanksale, J.N. Beltramini, J.A. Dumesic, Journal of Catalysis 258 (2008) 366–377.
[45] N. Ichikuni, Catalysis Letters 69 (2000) 33–36.
[46] J. Rynkowski, et al., Journal of the Chemical Society, Faraday Transactions 91 (1995) 3481–3484.
[47] J. Rynkowski, et al., Applied Catalysis A-General 106 (1993) 73–82.
[48] B. Scheffer, Applied Catalysis 46 (1989) 11–30.
[49] M. García-Diéguez, et al., Journal of Catalysis 270 (2010) 136–145.
[50] M. García-Diéguez, et al., Applied Catalysis A-General 377 (2010) 191–199.
[51] M. García-Diéguez, et al., Journal of Catalysis 274 (2010) 11–20.
[52] D. Briggs, M.P. Seah (Eds.), Practical Surface Analysis by Auger and X-Ray Photoelectron Spectroscopy, second ed., Wiley, Chichester, UK, 1990.
[53] L. Guczi, A. Sarkany, Z. Koppany, Applied Catalysis 120 (1994) L1.
[54] B. Pawelec, S. Damyanova, K. Arishtirova, J.L.G. Fierro, L. Petrov, Applied Catalysis A-General 323 (2007) 188–201.
[55] N.H.H. Abu Bakar, M.M. Bettahar, M. Abu Bakar, S. Monteverdi, J. Ismail, M. Alnot, Journal of Catalysis 265 (2009) 63–71.
[56] N.H.H. Abu Bakar, M.M. Bettahar, M. Abu Bakar, S. Monteverdi, J. Ismail, M. Alnot, Journal of Molecular Catalysis A: Chemical 308 (2009) 87–95.
[57] K. Lehnert, P. Claus, Catalysis Communications 9 (2008) 2543–2546.
[58] R.R. Davda, J.A. Dumesic, Angewandte Chemie International Edition 42 (2003) 4068–4071.
[59] N. Luo, F. Cao, X. Zhao, T. Xiao, D. Fang, Fuel 86 (2007) 1727–1736.
[60] J.W. Shabaker, R.D. Cortright, J.A. Dumesic, Journal of Catalysis 231 (2005) 67–76.